ARTICLE

# Polyelectrolyte Multilayer-Assisted Immobilization of Zero-Valent Iron Nanoparticles onto Polymer Nanofibers for Potential Environmental Applications

**Shili Xiao,[†,‡] Siqi Wu,[§] Mingwu Shen,[§] Rui Guo,[§] Qingguo Huang,*[,∥] Shanyuan Wang,[‡] and Xiangyang Shi*[,†,§]**

State Key Laboratory for Modification of Chemical Fibers and Polymer Materials, College of Textiles, and College of Chemistry, Chemical Engineering and Biotechnology, Donghua University, Shanghai 201620, People's Republic of China, and Department of Crop and Soil Sciences, University of Georgia, Griffin, Georgia 30223

**ABSTRACT** We report a facile approach to synthesizing and immobilizing zero-valent iron nanoparticles (ZVI NPs) onto polyelectrolyte (PE) multilayer-assembled electrospun polymer nanofibers for potential environmental applications. In this approach, negatively charged cellulose acetate (CA) nanofibers fabricated by electrospinning were assembled with multilayers of poly(diallyldimethylammonium chloride) (PDADMAC) and polyacrylic acid (PAA) through electrostatic layer-by-layer assembly. The formed PAA/PDADMAC multilayers onto CA nanofibers were then used as a nanoreactor to complex Fe(II) ions through the binding with the free carboxyl groups of PAA for subsequent reductive formation of ZVI NPs. Combined scanning electron microscopy, transmission electron microscopy, energy dispersive spectroscopy, Fourier transform infrared spectroscopy, and thermogravimetry analysis studies demonstrate that the ZVI NPs are successfully synthesized and uniformly distributed into the PE multilayers assembled onto the CA nanofibers. The produced hybrid nanofibrous mats containing ZVI NPs were found to exhibit superior capability to decolorize acid fuchsin, an organic dye in dyeing wastewater. We show that the loading capacity of ZVI NPs can be tuned by changing the number of PE layers and the cycles of binding/reduction process. Increasing the number of the binding/reduction cycles leads to a slight bigger size of the ZVI NPs, which is not beneficial for improving the reactivity of ZVI NPs. The present approach to synthesizing and immobilizing ZVI NPs onto polymer nanofibers opens a new avenue to fabricating various fiber-based composite materials with a high surface area to volume ratio for environmental, catalytic, and sensing applications.

**KEYWORDS:** layer-by-layer assembly • electrospinning • nanofibers • zero-valent iron nanoparticles • environmental applications

## INTRODUCTION

As a powerful and highly versatile approach to preparing functional nanostructured materials with tailored properties, layer-by-layer (LbL) self-assembly technique has received immense scientific and technological interest (1−3). The major advantage of the LbL technique is that the thickness, morphology, and composition of the targeted materials can be controlled by varying the number of the polymer deposition cycles and by changing the composition of the layer component (e.g., polyelectrolytes (PEs) (4), nanoparticles (NPs) (5), and precursor molecules (6), etc.). By utilizing the LbL assembly approach, a broad range of materials including polymers (7, 8), NPs (5), and biomolecules (9, 10) are able to be assembled onto various substrates (e.g., planar substrates, colloids, mesoporous particles, and membrane pores, etc.) to form functional nanostructured materials including, but not limited to, ultrathin polymer films (11), capsules (4, 12, 13), nanotubes (14, 15), and hollow spheres (16, 17). More importantly, PE multilayers assembled using PEs bearing carboxylic acid or amine groups can be used as nanoreactors to complex metal ions for the synthesis of inorganic NPs within the multilayers (16, 18−22). This nanoreactor concept was first discovered by Cohen and co-workers who utilized a block copolymer to synthesize PbS NPs (23) and later was co-developed by the groups of Cohen and Rubner to form NP-containing multilayer films and microcapsules (18−22). The functional nanomaterials developed using the LbL approach have been widely used in sensors (24), catalysts (25), environmental remediation (26, 27), and biomedical applications (7, 28, 29).

Zero-valent iron nanoparticles (ZVI NPs) have received considerable attention in their use as a cost-effective and environmentally benign agent for environmental remediation in the past decade. Many efforts have been devoted to the synthesis and application of ZVI NPs, especially exploring new approaches to mitigating their aggregation during the procedure of delivery and treatment (30−35). For instance,

* To whom correspondence should be addressed. E-mail: xshi@dhu.edu.cn (X.S.); qhuang@uga.edu (Q.H.).

Received for review August 31, 2009 and accepted October 16, 2009

† State Key Laboratory for Modification of Chemical Fibers and Polymer Materials, Donghua University.

‡ College of Textiles, Donghua University.

§ College of Chemistry, Chemical Engineering and Biotechnology, Donghua University.

∥ University of Georgia.

DOI: 10.1021/am900590j





Published on Web 10/26/2009

**Scheme 1. Schematic Illustration of Immobilizing ZVI NPs onto PE Multilayer-Assembled CA Nanofibers**

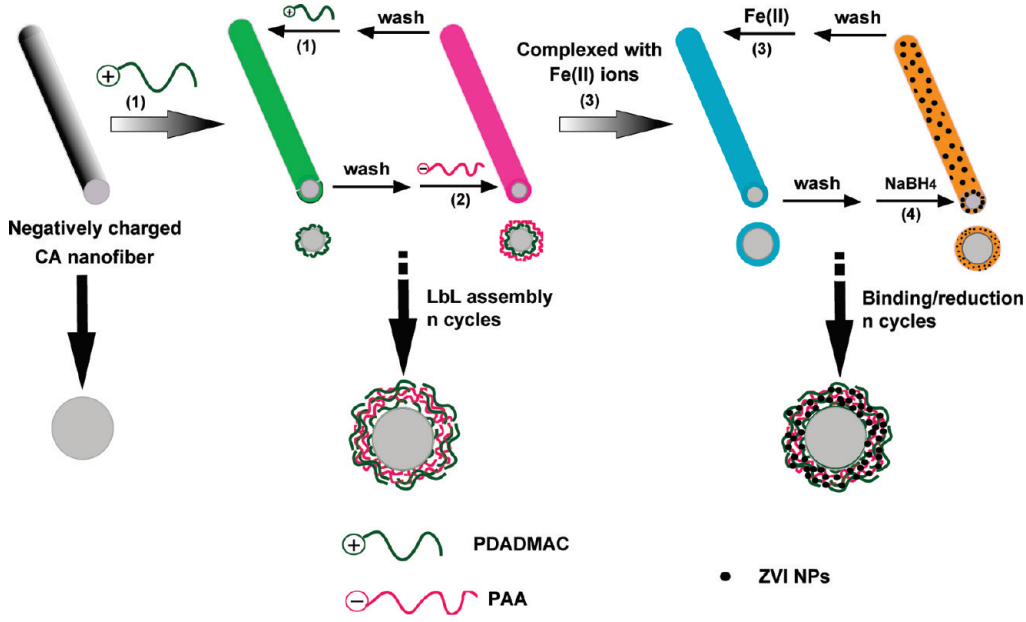


Sun et al. (34) prepared a stable dispersion of ZVI NPs using a nontoxic, biodegradable polymeric surfactant poly(vinyl alcohol-co-vinyl acetate-co-itaconic acid) as a dispersant. He and Zhao (33) used carboxymethyl cellulose as stabilizers to synthesize ZVI NPs with different sizes in order to prevent the NPs from agglomeration. Mallouk and co-workers (36) successfully synthesized ZVI NPs with a diameter of 10−30 nm on a nonporous, hydrophobic polymer resin support, which exhibit a high reactivity to remove toxic metal ion contaminants in aqueous solution. In our previous work, we immobilized ZVI NPs into PE multilayers assembled onto glass beads via an LbL assembly approach (27). The ZVI NPs immobilized onto the microparticle surfaces with controllable diameters displayed an excellent reactivity for the degradation of trichloroethylene. This implies that the LbL assembly approach provides a versatile tool to immobilize ZVI NPs onto microparticle carriers, which significantly improves the stability and effectiveness of the ZVI NPs for environmental applications. However, exploring new strategies to immobilize ZVI NPs onto various supports to meet specified requirements still remains a great challenge.

Recently, electrospinning technology has emerged as a relatively simple and popular approach for creating nanofibers with a high surface area to volume ratio. A broad range of organic, inorganic, and organic/inorganic hybrid nanostructured fiber-based materials have been fabricated for potential applications in sensors (37), catalysts (38−40), tissue engineering scaffolds (41), and filtration (42). To improve the functionality of the fiber materials, the versatile LbL assembly approach has been applied to assemble polymers or NPs onto the electrospun nanofibers (43−47). For instance, Müller et al. (45) functionalized electrospun polystyrene (PS) nanofibers with multilayered PEs, deoxyribonucleic acid oligonucleotides, and PE/gold NP composites via LbL assembly approach, respectively. Wang and coworkers (44) assembled a fluorescent probe, hydrolyzed poly[2-(3-thienyl) ethanol butoxy carbonyl-methyl urethane], onto the surface of cellulose acetate (CA) nanofibers to fabricate highly sensitive optical sensors. Zhang et al. (46) LbL-assembled titania NP/PE multilayers onto electrospun PS nanofibers, followed by dissolving the PS core fibers to form hollow titania-containing nanofibers with enhanced photocatalytic activity. It is anticipated that using the LbL assembly approach, one can fabricate ZVI NP-containing polymer nanofibrous mats with a high surface area to volume ratio, thereby providing a unique reactive filtration material for environmental remediation applications.

In this present study, we report the facile synthesis and immobilization of ZVI NPs onto a continuous nanofiber-based support with a high specific surface area through the combination of the LbL assembly approach with electrospinning technology. In this approach, electrospun CA nanofibers were LbL-assembled with multilayers of poly(diallyldimethylammonium chloride) (PDADMAC) and poly(acrylic acid) (PAA) through electrostatic interaction. Then, the PAA/PDADMAC multilayers coated onto the CA nanofibers were used as a nanoreactor to complex Fe(II) ions through the binding with the free carboxyl groups of PAA for subsequent reductive formation and immobilization of ZVI NPs (Scheme 1). Scanning electron microscopy (SEM), transmission electron microscopy (TEM), energy dispersive spectroscopy (EDS), Fourier transform infrared (FTIR) spectroscopy, and thermal gravimetric analysis (TGA) were utilized to characterize the morphology and composition of the ZVI NP-containing nanofibers. The decoloration efficiency of the ZVI NP-immobilized polymer nanofibers was examined using acid fuchsin as a model contaminant. We show that the developed ZVI NP-immobilized polymer nanofibers display an excellent reactivity toward decoloration of the model dye. To the best of our knowledge, this is the first report related to the combination of the LbL assembly approach with electrospinning technology to synthesize and immobilize ZVI

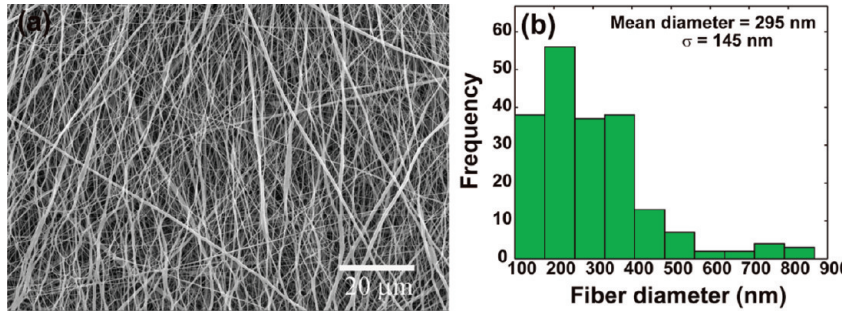


**FIGURE 1. SEM image (a) and diameter distribution histogram (b) of electrospun CA nanofibers.**

NPs for environmental applications. The major advantage of the developed approach lies in the feasibility to tune the size and loading of ZVI NPs onto the nanofibers, thereby providing a unique filtration material with tunable reactivity for environmental applications.

## EXPERIMENTAL SECTION

**Materials.** PAA (average $M_w$ = 240 000, 25 wt % in water) and PDADMAC (average $M_w$ = 100 000−200 000, 20 wt % in water) were obtained from Aldrich. Sodium borohydride was from J&K Chemical. $FeCl_2 \cdot 4H_2O$ and cellulose acetate (powder, viscosity 300.0−500.0 mPa s) were purchased from Sinopharm Chemicial Reagen Co., Ltd. Acetone and *N*,*N*-dimethylformamide (DMF) were obtained from Shanghai Boer Chemical Reagent Co., Ltd. Water used in all experiments was purified using a Milli-Q Plus 185 water purification system (Millipore, Bedford, MA) with resistivity higher than 18 MΩ cm.

**Fabrication of CA Nanofibers.** CA nanofibers were fabricated by electrospinning a 12 g/L CA solution according to a procedure described in the literature with slight modification (43). The CA solution was prepared by dissolving a measured amount of CA powder in a mixed solvent of acetone and DMF (2/1 v/v) for 12 h with vigorous stirring. Freshly prepared CA solution (10 mL) was loaded into a syringe with a needle having an inner diameter of 0.8 mm. The feed rate was controlled by a syringe pump at 1.0 mL/h. The applied voltage was kept at 20 kV, and the tip to collector distance was set at 20 cm.

**Synthesis of ZVI NP-Immobilized Composite Nanofibers (Scheme 1).** PAA/PDADMAC multilayers were LbL-assembled onto the fabricated CA nanofibers. PDADMAC and PAA solutions used for deposition were prepared in water (containing 0.5 M NaCl) with a concentration of 2 mg/mL. The pH value of both solutions was adjusted to 3.5 using 1 M HCl or 1 M NaOH. This pH value has been proved to allow the effective binding of metal ions for subsequent formation of NPs in previous work (19, 22, 27). The negatively charged CA nanofibers (43) enabled the deposition of positively charged PDADMAC as the first layer. In a typical procedure, the CA nanofibrous mats were first immersed into PDADMAC solution for 5 min, followed by rinsing with water three times (each rinsing step took 2 min). Then, the substrates were immersed in the negatively charged PAA solution for 5 min, followed by similar rinsing steps in water. The immersion/rinsing cycles were repeated until the desired number of bilayers was achieved. The PE multilayers thus obtained were denoted as $(PAA/PDADMAC)_n$. Each assembly of a PAA layer followed by a PDADMAC layer was defined as a bilayer, and the first layer of PDADMAC was regarded as a base layer and was not included in the bilayers in our naming system.

The PE multilayer-assembled CA nanofibrous mats were then immersed into an aqueous solution of ferrous chloride (0.18 M) for 30 min to allow Fe(II) ions to complex with available free carboxyl groups of PAA through ionic exchange, followed by three rinses with water. Sodium borohydride solution (0.36 M) was dropped gradually onto the nanofibrous mats complexed with Fe(II) ions until there were no bubbles of hydrogen gas produced. The cycle of binding and reduction of Fe(II) ions was repeated to form additional ZVI NPs. Finally, the formed ZVI NP-immobilized composite mats were rinsed three times with water, vacuum-dried at room temperature for 24 h, and stored in a desiccator before use.

**Characterization.** Morphologies of the electrospun pure CA nanofibrous mats and PE multilayer-coated mats with different numbers of bilayers were observed using SEM (JSM-5600LV, JEOL Ltd., Japan) with an operating voltage of 10 kV. The elemental composition of the samples was analyzed by EDS (IE 300X, Oxford, U.K.) attached to the SEM at an operating voltage of 15 kV. The cross-sectional images of the ZVI NP-containing nanofibrous mats were imaged using TEM (JEM2100, JEOL Ltd., Japan) with an operating voltage of 200 kV. The diameters of nanofibers and particle sizes were measured using image analysis software ImageJ 1.40G (http://rsb.info.nih.gov/ij/download.html). At least 200 randomly selected nanofibers or ZVI NPs in different SEM or TEM images were analyzed for each sample in order to acquire the diameter/size distribution histograms. TGA was carried out on a TG 209 F1 (NETZSCH Instruments Co., Ltd., Germany) thermogravimetric analyzer with a heating rate of 10 °C/min in air. FTIR spectra were recorded using a Nicolet 5700 spectrometer (Thermo Nicolet Corp.) at a wavenumber range of 4000−500 $cm^{-1}$ under ambient conditions.

**Acid Fuchsin Decoloration.** Acid fuchsin was selected as a model species to prepare the dye-contaminated water. An aliquot of acid fuchsin aqueous solution (60 mg/L, 30 mL) with a pH value of 6.8 was filled into a 50 mL beaker. Then, a ZVI NP-immobilized nanofibrous mat with a final Fe concentration of 0.15 g/L was added into the beaker, followed by gentle magnetic stirring at room temperature. At each time interval, 1 mL of the aqueous sample was withdrawn and diluted to 2.5 mL with water for the analysis of acid fuchsin decoloration efficiency by a Lambda-25 UV-vis spectrometer (Perkin-Elmer Co.). The decoloration percentage of acid fuchsin was calculated according to the equation

$$\text{decoloration} = \frac{C}{C_0} \times 100\% \qquad (1)$$

where $C_0$ is the initial concentration of acid fuchsin and $C$ is the concentration of acid fuchsin after treatment with nanofibers at a given time point.

## RESULTS AND DISCUSSION

**Fabrication of CA and PAA/PDADMAC Multilayer-Assembled CA Nanofibrous Mats.** Under the selected experimental conditions, smooth and continuous CA nanofibers with random orientation were produced

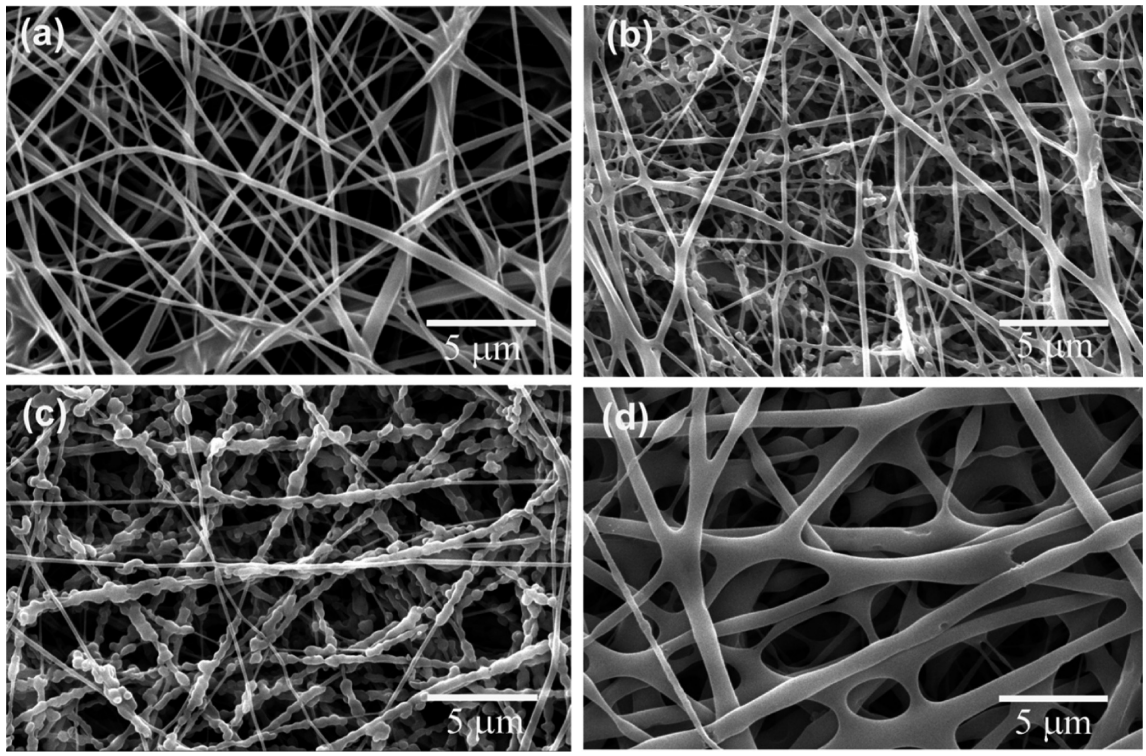


**FIGURE 2. SEM images of CA nanofibers assembled with (a) three, (b) four, (c) five, and (d) six bilayers of PAA/PDADMAC.**

with a mean diameter of 295 ± 145 nm (Figure 1). The electrospun CA nanofibrous mats exhibit a three-dimensional structure with pores in micrometer and sub-micrometer size, which is a typical feature for electrospun polymer nanofibrous mats.

The electrospun CA nanofibrous mats were then LbL-assembled with PAA/PDADMAC multilayers in order to fabricate the nanoreactor for subsequent formation of ZVI NPs. The assembly process involves the alternate deposition of oppositely charged polymer layers onto each individual nanofiber. To render the final formed PE multilayer-coated CA nanofibrous mats with porous structure for future application as a filtration material, the number of PE multilayers deposited onto the CA nanofibrous mat was optimized. The CA nanofibrous mats were deposited with 3, 4, 5, 6, 9, and 18 bilayers of PAA/PDADMAC, respectively. SEM morphological studies (Figure 2) showed that the fiber shape and porous structured nanofibrous mats were well maintained when the number of the assembled PAA/PDADMAC bilayers was below six. It is clear that a relatively thin (three bilayers) or thick (six bilayers) coating of PAA/PDADMAC multilayers onto CA nanofibers generates a smooth morphology (Figure 2a,d), while the intermediate coating (four or five bilayers) forms nanofibrous mats with some pearl necklace like structures (Figure 2b,c). The formation of the pearl necklace like structured fibers might be caused by the nonsaturated deposition (5 min) of the coiled structure of PAA and PDADMAC in sodium chloride solution (9). However, when the deposition number of bilayers was increased up to nine, an obvious ball-like structure appeared and seemed to accumulate inside the pores between the nanofibers. In addition, the pores began to be blocked (Figure S1a, Supporting Information). The CA nanofibrous mats coated with $(PAA/PDADMAC)_{18}$ could not maintain the porous fibrous structure and exhibited a planar membrane-like structure (Figure S1b, Supporting Information). This can be explained as follows: during the process of LbL self-assembly, the PE multilayers are not only assembled onto the surface of each individual nanofibers but also assembled onto the fiber junction site. The coverage of PE multilayers onto either the surface of individual fibers or the surface of the fiber junction site could have approached to nearly 100% as the PE deposition cycles increased. With the increase of the number of the polymer deposition cycles, the PE multilayer films ultimately fill the limited space among the adjacent nanofibers (48). Therefore, six bilayers of PAA/PDADMAC were chosen to coat onto the CA nanofibrous mats and were used as a nanoreactor to immobilize ZVI NPs (see below). The thickness of the six-bilayer coating of PAA/PDADMAC could be estimated to be 12 nm according to the literature (49). The PE coatings were stable at room temperature for at least 6 months.

**Synthesis and Characterization of ZVI NP-Containing Polymer Nanofibrous Mats.** The $(PAA/PDADMAC)_6$-coated CA nanofibrous mats were immersed into ferrous solution to complex the Fe(II) ions with carboxyl groups of PAA for subsequent formation of ZVI NPs. Upon addition of the reducing agent $NaBH_4$, ZVI NPs were formed and immobilized onto the polymer nanofibrous mats. SEM, TEM, EDS, FTIR, and TGA were used to characterize the ZVI NP-containing CA nanofibrous mats.

SEM morphology of the ZVI NP-immobilized CA nanofibers formed by two cycles of binding and reduction of Fe(II) ions (Figure 3a) shows that the hybrid nanofibrous mats still

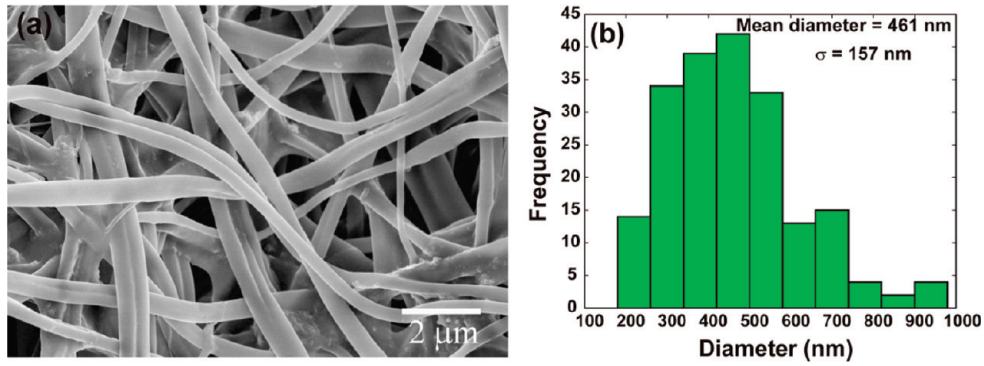


FIGURE 3. SEM image (a) and diameter distribution histogram (b) of ZVI NP-immobilized CA nanofibrous mats. The ZVI NPs were immobilized within $(PAA/PDADMAC)_6$ multilayers assembled onto CA fibrous mats by two cycles of binding/reduction processes.

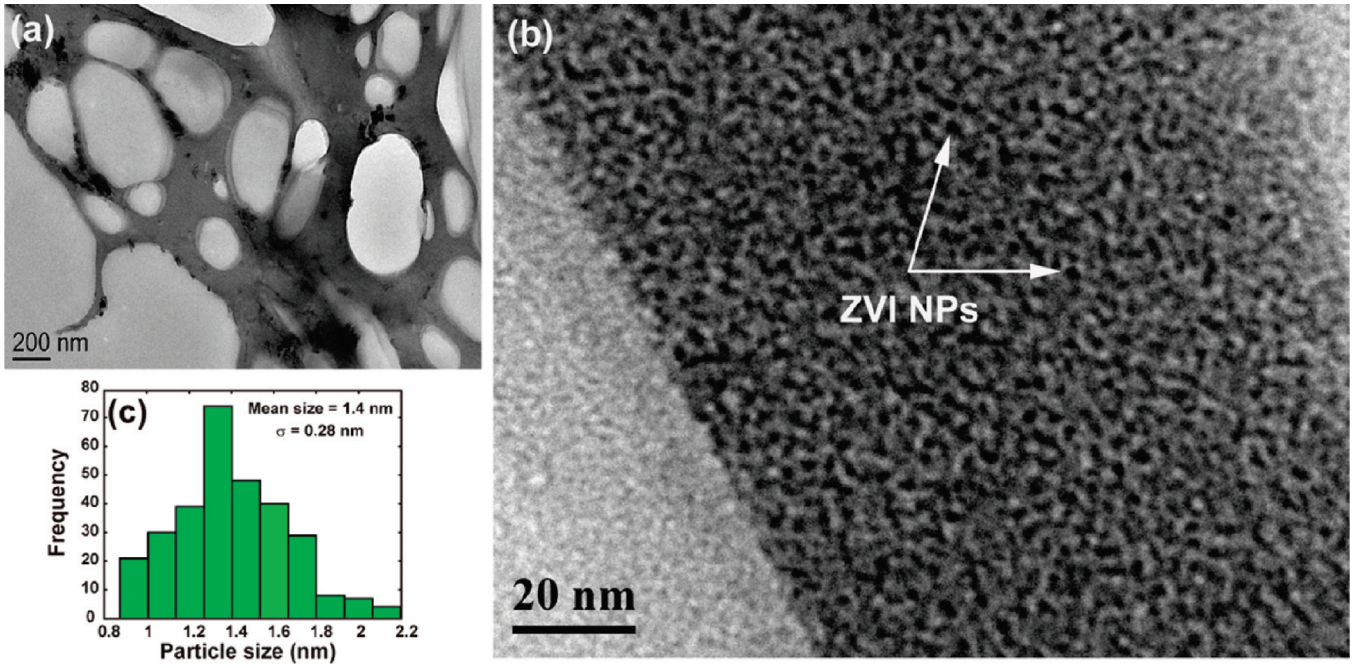


FIGURE 4. Cross-sectional TEM images of ZVI NP-immobilized CA nanofibrous mats (shown in Figure 3): (a) overview of the TEM image; (b) magnified TEM image showing the individual ZVI NPs; (c) size distribution histogram of the formed ZVI NPs.

exhibit a typical, porous nanofibrous structure with a smooth surface. This suggests that the ZVI NPs thus synthesized are uniformly immobilized into the $(PAA/PDADMAC)_6$ multilayers coated onto CA nanofibrous mats. In comparison with the pristine CA nanofibers (Figure 1b), the ZVI NP-containing CA nanofibers have a larger mean diameter (461 ± 157 nm), which is caused by the deposition of PE mulitlayers and the immobilization of ZVI NPs. The cross-sectional TEM images (Figure 4a,b) indicate that the ZVI NPs are dispersed in the PE multilayer film deposited onto the CA nanofibers and have a relatively dense and uniform distribution (see the dark contrast of the cross section of the PE multilayers). The size (mean ± std) of the ZVI NPs was estimated to be 1.4 ± 0.3 nm (Figure 4c). The elemental iron signals in the EDS spectrum (Figure 5) demonstrated that ZVI NPs were successfully synthesized and immobilized onto the PE multilayer-assembled CA nanofibers. The presence of element iron and oxygen is consistent with the iron/iron oxide core–shell structure reported in the literature (27, 50). Part of the element oxygen is also ascribed to the CA polymers

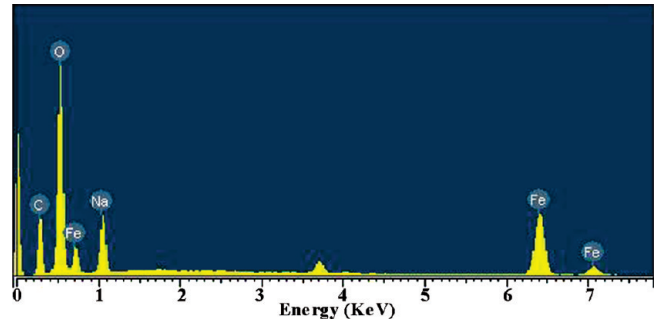


FIGURE 5. EDS spectrum of ZVI NP-immobilized CA nanofibers (shown in Figure 3).

and the carboxyl groups of PAA. The sodium signal was from the sodium borohydride residue used for ferrous reduction.

The formation of ZVI NPs in the composite nanofibers was further confirmed using FTIR spectroscopy (Figure 6). The FTIR spectra of $(PAA/PDADMAC)_6$-assembled CA nanofibrous mats before and after immobilization of ZVI NPs (after two cycles of binding/reduction processes) show a significant difference. A strong adsorption peak at 1700 $cm^{-1}$ assigned

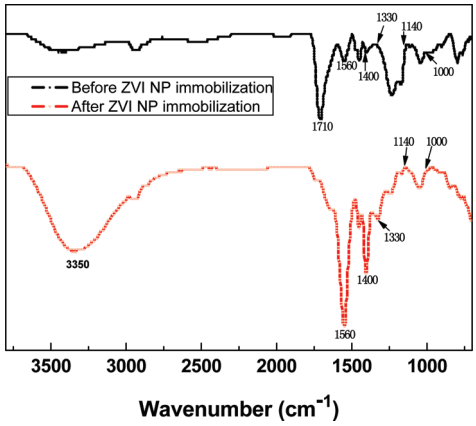


**FIGURE 6. FTIR spectra of $(PAA/PDADMAC)_6$-assembled CA nanofibrous mats before and after immobilization of ZVI NPs by two cycles of binding/reduction.**

to the free carboxylic group (COO− asymmetric stretching) of PAA in the LbL film before iron loading disappeared and shifted to 1560 $cm^{-1}$ (C═O asymmetric vibrations in the carboxylate) after iron loading, in agreement with literature data (51). Changes at 1400 $cm^{-1}$, in the regions of 1330−1140 $cm^{-1}$ (C−O stretching) and 1000−804 $cm^{-1}$, indicate the interaction between ZVI NPs and the PAA carboxyl groups. Moreover, a very broad absorption band in the region of 3690−1780 $cm^{-1}$ for both samples indicates the presence of a tiny amount of water molecules because the PE multilayer films assembled on the CA nanofibers can easily absorb moisture in air (52). In general, after introduction of ZVI NPs into the composite fibrous mats, the spectral features of the nanofibers seem to be broader, consistent with literature data (51).

The advantage of using PE multilayers as nanoreactors lies in the possibility of tuning the particle size by varying the number of the binding/reduction cycles (16, 18−22, 27). In this study, the effect of the number of binding/reduction cycles on the particle size was investigated. The loaded ZVI NPs with different sizes may be essential for further optimization of their capacity for environmental remediation. In comparison with the ZVI NPs prepared with two cycles of binding and reduction (1.4 nm, Figure 4), the ZVI NPs prepared with six cycles of binding and reduction under similar conditions have a larger mean size of 2.3 ± 0.5 nm (Figure S2, Supporting Information). It suggests that the particle size of ZVI NPs can be tuned by varying the number of binding/reduction cycles, which is consistent with the literature (22, 27).

Iron loading in the composite nanofibrous mats prepared under various conditions was estimated by TGA (Tables 1 and 2). For the case of two cycles of binding and reduction processes, the iron loading percentage increased with the number of PE bilayers deposited onto the electrospun CA nanofibers (Table 1). A sharp increase was observed at four bilayers (15.5 ± 1.76%) in comparison to that at three bilayers (9.0 ± 0.79%). On further increasing the number of bilayers to five or six, the iron loading was leveled off. Table 2 gives the iron loading percentages on $(PAA/PDADMAC)_6$-assembled CA fibrous mats with the number of

**Table 1. Iron Loading Percentages on the CA Nanofibrous Mats Assembled with Different Numbers of PAA/PDADMAC Bilayers Prepared by Two Cycles of Binding/Reduction**

| no. of PE bilayers | iron loading (%) |
|---|---|
| 3 | 9.0 ± 0.79 |
| 4 | 15.5 ± 1.76 |
| 5 | 18.3 ± 0.75 |
| 6 | 19.2 ± 0.56 |

**Table 2. Iron Loading Percentages on the $(PAA/PDADMAC)_6$-Assembled CA Nanofibrous Mats Prepared by Different Cycles of Binding/Reduction**

| no. of binding/reduction cycles | iron loading (%) |
|---|---|
| 2 | 19.2 ± 0.56 |
| 4 | 22.7 ± 0.55 |
| 6 | 32.1 ± 0.96 |

binding/reduction cycles. It is clear that the iron loading percentage increases with an increase of the number of binding/reduction cycles. This is because after a reaction cycle to form ZVI NPs, the carboxylic acid groups of PAA are available again for the next cycle of Fe(II) ion binding and reduction, in agreement with literature data (22, 27). Our results confirm that the loading and size of ZVI NPs immobilized onto polymer nanofibers could be controlled by manipulating the synthesis conditions, similar to those formed onto microparticles (27).

**Acid Fuchsin Decoloration.** ZVI NPs have been used to decolorize some dyes in dyeing wastewater (35). To explore the potential environmental applications, we selected acid fuchsin, a common organic dye in the textile industry, as a model contaminant in dyeing wastewater to test the remediation capability of ZVI NP-immobilized polymer nanofibrous mats. The experiment for acid fuchsin (concentration 60 mg/L) decoloration was monitored using UV−vis spectroscopy. For the ZVI NP-immobilized nanofibrous mats prepared with two cycles of binding/reduction, we showed that the intensity of the characteristic absorption peak of acid fuchsin at 544 nm suddenly decreased after 5 min exposure of the mat to the acid fuchsin solution. When the exposure time was extended to 40 min, gradual decoloration was observed (Figure 7a). The result is consistent with the observation in Figure 7c. A detailed molecular mechanism regarding the decoloration of acid fuchsin using ZVI NPs is still unclear. We think that the chromophore of acid fuchsin is able to be destroyed after the iron reduction process, similar to what is found from literature data (35, 53).

The remediation capability of ZVI NPs is size-dependent (27). The ZVI NPs immobilized onto CA fibers with a larger size (2.3 nm) synthesized with six binding/reduction cycles were also examined for comparison with those with a smaller size (1.4 nm) synthesized with two binding/reduction cycles. In both cases, a similar iron weight was used. It is clear that the 2.3 nm ZVI NPs immobilized onto the CA nanofibrous mats exhibit lower reactivity toward the decoloration of acid fuchsin, as illustrated by UV−vis absorption curves and photos at different time intervals (Figure 7b,d),

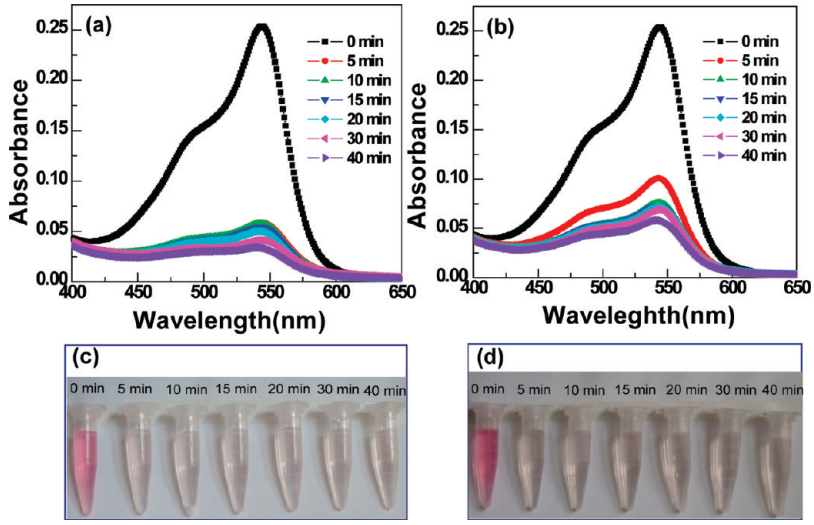


FIGURE 7. UV−vis spectra of a solution of acid fuchsin (60 ml/L, 30 mL) in the presence of ZVI NP- immobilized hybrid nanofibrous mats synthesized with two (a) and six (b) cycles of binding/reduction at a time interval of 0, 5, 10, 15, 20, 30, and 40 min, respectively, and photos of the acid fuchsin solution treated with ZVI NP-immobilized hybrid nanofibrous mats synthesized with two (c) and six (d) cycles of binding/reduction at different time intervals.

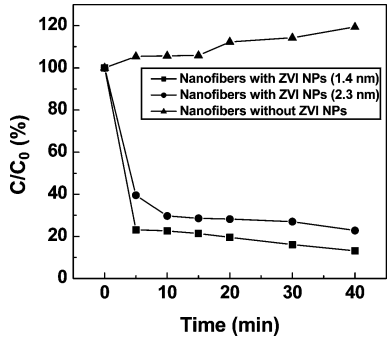


FIGURE 8. Remaining fraction of acid fuchsin over time after treatment with ZVI NP-immobilized hybrid nanofibrous mats with ZVI NP sizes of 1.4 and 2.3 nm, respectively.

respectively. The smaller size and greater specific surface area of the ZVI NPs obtained with two cycles of binding/reduction were in some large measure responsible for reactivity greater than those prepared with six cycles of binding/reduction. The better remediation capability of ZVI NPs (1.4 nm) immobilized onto CA nanofibers was also demonstrated by plotting the percentage of decoloration as a function of exposure time (Figure 8). In comparison with the decoloration efficiency of ZVI NPs synthesized with six cycles of binding/reduction (77.2%), the ultimate decoloration efficiency of those synthesized with 2 cycles of binding/reduction could be up to 86.8%. We note that the decoloration effect of the ZVI NP-immobilized CA nanofibers is solely related to the immobilized ZVI NPs. A control experiment using PE multilayered CA nanofibers without the ZVI NPs does not show the effect of acid fuchsin decoloration (Figure 8). The slightly increased $C/C_0$ value with time in this case is believed to be related to the water absorption of the fibrous mats with time, which slightly concentrates the original acid fuchsin solution. In addition, the ZVI NP-containing polymer nanofibrous mats are easily reusable and recyclable. We chose to evaluate the reusability of the nanofibrous mat with 1.4 nm ZVI NPs immobilized, since this mat displayed decoloration capability higher than that immobilized with 2.3 nm ZVI NPs. After treatment with sodium borohydride for 10 min, the renewed ZVI NP-containing nanofibrous mat still performed well for the second and third decoloration experiments (Figure S3, Supporting Information).

The major advantage of the ZVI NP-immobilized polymer nanofibers is that the fibrous mats can be easily separated from the contaminated water, which is ideal for them to be used as a reusable and recyclable filtration material. In addition, inductively coupled plasma atomic emission spectroscopy studies show that the immobilized ZVI NPs are quite stable and do not escape from the fibrous mats during the remediation process and during the storage in water for 1 month at room temperature. In comparison with the colloidal ZVI NPs synthesized using a conventional approach (54), this material does not lead to secondary contamination when exposed to water, which is quite useful for their environmental remediation applications.

## CONCLUSION

In summary, we have successfully developed a facile approach to synthesizing and immobilizing ZVI NPs onto polymer nanofibers. The PE multilayer nanoreactors assembled onto polymer nanofibers allow the formation of ZVI NPs with tunable sizes and iron loading. The ZVI NP-immobilized nanofibrous mats were demonstrated to be able to decolorize an organic dye, acid fuchsin, a model contaminant in dyeing wastewater, and the decoloration percentage could be up to 86.8% within 40 min. The remarkable remediation capability of the hybrid fibrous mats is mainly attributed to the small size of ZVI NPs (1.4 nm) uniformly immobilized into the PE mulilayered CA nanofibers. In addition, the porous polymer nanofibrous mats with a high surface area to volume ratio should allow an efficient contact and interaction with the contaminants, which is highly useful for practical environmental applications. We anticipate that the as-prepared ZVI NP-immobilized hybrid

nanofibrous mats can be applicable in the remediation of many other contaminants such as trichloroethylene, polychlorinated biphenyls, and toxic metal ions (e.g. Cr(VI)). The related experiments are currently being carried out in our laboratory. Furthermore, the developed approach to immobilizing ZVI NPs onto polymer nanofibers with tunable size and loading percentage may also be extended for tailoring the size, composition, and surface properties of other three-dimensional porous nanostructured materials with a high surface area for various applications, including but not limited to catalysis, sensing, environmental remediation, and biomedicine.

**Acknowledgment.** This research is financially supported by the State Key Laboratory for Modification of Chemical Fibers and Polymer Materials, the Shanghai Pujiang program (No. 09PJ1400600), the Program for Professor of Special Appointment (Eastern Scholar) at Shanghai Institutions of Higher Learning, and the National Basic Research Program of China (973 Program, 2007CB936000). The Shanghai Bai Yu Lan Foundation (No. 2009B011) is acknowledged for supporting the collaboration between Donghua University and the University of Georgia.

**Supporting Information Available:** Figures giving additional SEM images of PE multilayer-assembled CA nanofibers, cross-sectional TEM images of ZVI NP-immobilized CA nanofibers synthesized with six cycles of binding/reduction, a size distribution histogram of the formed ZVI NPs, and an evaluation of the reusability of the polymer nanofibrous mats containing 1.4 nm ZVI NPs. This material is available free of charge via the Internet at http://pubs.acs.org.

## REFERENCES AND NOTES

(1) Decher, G.; Hong, J. D. *Ber. Bunsen-Ges. Phys. Chem.* **1991**, *95*, 1430–1434.
(2) Decher, G. *Science* **1997**, *277*, 1232–1237.
(3) Decher, G.; Schlenoff, J. B. *Multilayer Thin Films: Sequential Assembly of Nanocomposite Materials*; Wiley-VCH: Weinheim, Germany, 2003.
(4) Donath, E.; Sukhorukov, G. B.; Caruso, F.; Davis, S. A.; Mohwald, H. *Angew. Chem., Int. Ed.* **1998**, *37*, 2201–2205.
(5) Srivastava, S.; Kotov, N. A. *Acc. Chem. Res.* **2008**, *41*, 1831–1841.
(6) Caruso, F.; Shi, X.; Caruso, R.; Susha, A. *Adv. Mater.* **2001**, *13* (10), 740–744.
(7) Shi, X.; Wang, S.; Chen, X.; Meshinchi, S.; Baker, J. R., Jr. *Mol. Pharm.* **2006**, *3*, 144–151.
(8) Wang, S. H.; Shi, X.; Chen, X.; Baker, J. R., Jr. *Macromol. Biosci.* **2009**, *9*, 429–436.
(9) Shi, X.; Sanedrin, R. J.; Zhou, F. *J. Phys. Chem. B* **2002**, *106*, 1173–1180.
(10) Caruso, F.; Moehwald, H. *J. Am. Chem. Soc.* **1999**, *121*, 6039–6046.
(11) Hajicharalambous, C. S.; Lichter, J.; Hix, W. T.; Swierczewska, M.; Rubner, M. F.; Rajagopalan, P. *Biomaterials* **2009**, *30*, 4029–4036.
(12) Shi, X.; Briseno, A. L.; Sanedrin, R. J.; Zhou, F. *Macromolecules* **2003**, *36*, 4093–4098.
(13) Wang, Y.; Angelatos, A. S.; Caruso, F. *Chem. Mater.* **2008**, *20*, 848–858.
(14) Ai, S.; Lu, G.; He, Q.; Li, J. *J. Am. Chem. Soc.* **2003**, *125*, 11140–11141.
(15) Shi, X.; Han, S.; Sanedrin, R. J.; Galvez, C.; Ho, D. G.; Hernandez, B.; Zhou, F.; Selke, M. *Nano Lett.* **2002**, *2*, 289–293.
(16) Shi, X.; Shen, M.; Moehwald, H. *Prog. Polym. Sci.* **2004**, *29*, 987–1019.
(17) Caruso, F.; Caruso, R. A.; Mohwald, H. *Science* **1998**, *282*, 1111–1114.
(18) Chia, K.-K.; Cohen, R. E.; Rubner, M. F. *Chem. Mater.* **2008**, *20*, 6756–6763.
(19) Joly, S.; Kane, R.; Radzilowski, L.; Wang, T.; Wu, A.; Cohen, R. E.; Thomas, E. L.; Rubner, M. F. *Langmuir* **2000**, *16* (3), 1354–1359.
(20) Lee, D.; Cohen, R. E.; Rubner, M. F. *Langmuir* **2005**, *21*, 9651–9659.
(21) Lee, D.; Rubner, M. F.; Cohen, R. E. *Chem. Mater.* **2005**, *17*, 1099–1105.
(22) Wang, T. C.; Rubner, M. F.; Cohen, R. E. *Langmuir* **2002**, *18*, 3370–3375.
(23) Kane, R. S.; Cohen, R. E.; Silbey, R. *Chem. Mater.* **1996**, *8*, 1919–1924.
(24) Qi, W.; Yan, X.; Duan, L.; Cui, Y.; Yang, Y.; Li, J. *Biomacromolecules* **2009**, *10*, 1212–1216.
(25) Kidambi, S.; Dai, J.; Li, J.; Bruening, M. L. *J. Am. Chem. Soc.* **2004**, *126*, 2658–2659.
(26) Krogman, K. C.; Zacharia, N. S.; Grillo, D. M.; Hammond, P. T. *Chem. Mater.* **2008**, *20*, 1924–1930.
(27) Huang, Q.; Shi, X.; Pinto, R. A.; Petersen, E.; Weber, W. J., Jr. *Environ. Sci. Technol.* **2008**, *42*, 8884–8889.
(28) Qi, W.; Yan, X.; Fei, J.; Wang, A.; Cui, Y.; Li, J. *Biomaterials* **2009**, *30*, 2799–2806.
(29) Tang, Z.; Wang, Y.; Podsiadlo, P.; Kotov, N. A. *Adv. Mater.* **2006**, *18*, 3203–3224.
(30) He, F.; Zhao, D. *Environ. Sci. Technol.* **2005**, *39*, 3314–3320.
(31) Li, X.-Q.; Elliott, D. W.; Zhang, W.-X. *Crit. Rev. Solid State Mater. Sci.* **2006**, *31* (4), 111–122.
(32) Darab, J. G.; Amonette, A. B.; Burke, D. S. D.; Orr, R. D.; Ponder, S. M.; Schrick, B.; Mallouk, T. E.; Lukens, W. W.; Caulder, D. L.; Shuh, D. K. *Chem. Mater.* **2007**, *19*, 5703–5713.
(33) He, F.; Zhao, D. *Environ. Sci. Technol.* **2007**, *41*, 6216–6221.
(34) Sun, Y.-P.; Li, X.-Q.; Zhang, W.-X.; Wang, H. P. *Colloids Surf., A* **2007**, *308*, 60–66.
(35) Epolito, W. J.; Yang, H.; Bottomley, L. A.; Pavlostathis, S. G. *J. Hazard. Mater.* **2008**, *160*, 594–600.
(36) Ponder, S. M.; Darab, J. G.; Bucher, J.; Caulder, D.; Craig, I.; Davis, L.; Edelstein, N.; Lukens, W.; Nitsche, H.; Rao, L.; Shuh, D. K.; Mallouk, T. E. *Chem. Mater.* **2001**, *13*, 479–486.
(37) Wang, X.; Drew, C.; Lee, S.-H.; Senecal, K. J.; Kumar, J.; Samuelson, L. A. *Nano Lett.* **2002**, *2*, 1273–1275.
(38) Drew, C.; Liu, X.; Ziegler, D.; Wang, X.; Bruno, F. F.; Whitten, J.; Samuelson, L. A.; Kumar, J. *Nano Lett.* **2003**, *3*, 143–147.
(39) Chronakis, I. S. *J. Mater. Process. Technol.* **2005**, *167*, 283–293.
(40) Hong, Y.; Li, D.; Zheng, J.; Zou, G. *Nanotechnology* **2006**, *17*, 1986–1993.
(41) Zhu, X.; Cui, W.; Li, X.; Jin, Y. *Biomacromolecules* **2008**, *9*, 1795–1801.
(42) Yoon, K.; Hsiao, B. S.; Chu, B. *J. Mater. Chem.* **2008**, *18*, 5326–5334.
(43) Ding, B.; Kim, J.; Kimura, E.; Shiratori, S. *Nanotechnology* **2004**, *15*, 913–917.
(44) Wang, X.; Kim, Y.-G.; Drew, C.; Ku, B.-C.; Kumar, J.; Samuelson, L. A. *Nano Lett.* **2004**, *4*, 2004.
(45) Muller, K.; Quinn, J. F.; Johnston, A. P. R.; Becher, M.; Greiner, A.; Caruso, F. *Chem. Mater.* **2006**, *18*, 2397–2403.
(46) Zhang, T.; Ge, L.; Wang, X.; Gu, Z. *Polymer* **2008**, *49*, 2898–2902.
(47) Lee, J. A.; Krogman, K. C.; Ma, M.; Hill, R. M.; Hammond, P. T.; Rutledge, G. C. *Adv. Mater.* **2009**, *21*, 1252–1256.
(48) Ding, B.; Fujimoto, K.; Shiratori, S. *Thin Solid Films* **2005**, *491*, 23–28.
(49) Elzbieciak, M.; Kolasinska, M.; Warszynski, P. *Colloids Surf., A* **2008**, *321*, 258–261.
(50) Martin, J. E.; Herzing, A. A.; Yan, W.; Li, X.; Koel, B. E.; Kiely, C. J.; Zhang, W. *Langmuir* **2008**, *24*, 4329–4334.
(51) Nesterova, M. V.; Walton, S. A.; Webb, J. *J. Inorg. Biochem.* **2000**, *79*, 109–118.
(52) Hao, E.; Lian, T. *Langmuir* **2000**, *16*, 7879–7881.
(53) Fan, J.; Guo, Y.; Wang, J.; Fan, M. *J. Hazard. Mater.* **2009**, *166*, 904–910.
(54) Wang, C.-B.; Zhang, W.-X. *Environ. Sci. Technol.* **1997**, *31*, 2154–2156.

AM900590J